

Superconductivity of alkali-metal intercalated BC_2

Cite as: AIP Advances **10**, 065213 (2020); <https://doi.org/10.1063/5.0008280>

Submitted: 21 March 2020 . Accepted: 23 May 2020 . Published Online: 10 June 2020

Wataru Hayami , and Takaho Tanaka



View Online



Export Citation



CrossMark



NEW: TOPIC ALERTS

Explore the latest discoveries in your field of research

SIGN UP TODAY!

Superconductivity of alkali-metal intercalated BC₂

Cite as: AIP Advances 10, 065213 (2020); doi: 10.1063/5.0008280

Submitted: 21 March 2020 • Accepted: 23 May 2020 •

Published Online: 9 June 2020



Wataru Hayami^{a)}  and Takaho Tanaka

AFFILIATIONS

International Center for Materials Nanoarchitectonics, National Institute for Materials Science, 1-1 Namiki, Tsukuba, Ibaraki 305-0044, Japan

^{a)} Author to whom correspondence should be addressed: HAYAMI.Wataru@nims.go.jp

ABSTRACT

The superconductivity of alkali-metal intercalated BC₂, M_xBC₂ (M = Li, Na, and K; $x = 0.5$ – 1.5), has been studied using first-principles calculations. The calculated critical temperature (T_c) values are substantially high at $x = 0.5$ (49.8–57.1 K), which are higher than those for MgB₂ and close to those predicted for Li_xB_yC_z compounds. The T_c values at $x = 1.5$ are comparatively low (0.6–5.6 K) and close to those for graphite intercalation compounds. No superconductivity is observed at $x = 1.0$ for all alkali metals. An analysis of the electronic structures reveals that at $x = 0.5$, the state at the Fermi energy includes the σ bond character. In contrast, at $x = 1.5$, the state includes only π bonds comprising p_z orbitals of B and C atoms. The σ bond character is essential for attaining high T_c values because the σ bond couples strongly with the bending-like phonon modes of the BC₂ layer. However, the π bond couples weakly with the stretching-like phonon modes due to the small overlap of the p_z orbitals, which results in a relatively low T_c for the material.

© 2020 Author(s). All article content, except where otherwise noted, is licensed under a Creative Commons Attribution (CC BY) license (<http://creativecommons.org/licenses/by/4.0/>). <https://doi.org/10.1063/5.0008280>

I. INTRODUCTION

Graphite and graphite-related materials have been studied and utilized for centuries. Since a technique for exfoliating single-layer graphene was developed,¹ graphite and graphite-related materials have been attracting more attention than ever. Most of the unique properties of these substances derive from two-dimensional atomic structures and the semi-metallic electronic structures that distinguish them from three-dimensional bulk materials.

Based on the B–C binary phase diagram,² the substitution of carbon in graphite with boron is allowed only by a few atomic percent, which means that graphite-like (g -) B _{x} C _{y} is thermodynamically unfavorable. However, syntheses of g -BC _{x} ($x = 3$ – 9) via chemical vapor deposition,^{3–7} the arc-discharge method,⁸ and segregation onto a metal diboride surface⁹ have been reported as a metastable phase. It appears that experimentally, the value of x cannot be smaller than three, i.e., the composition ratio of B is limited to 25 at. %. This is understandable based on the fact that the electronic structure of graphite has the Fermi level in the middle of the pseudogap (semi-metallic); hence, the substitution with B atoms reduces electrons in the bonding orbitals.

Consequently, g -BC and g -BC₂ are yet to be synthesized. However, these structures appear in compounds such as M _{x} B _{y} C _{z} in which the metal atoms M stabilize the BC _{x} layer by donating electrons. It has been established that g -BC is formed in LiBC and MgB₂C₂,^{10,11} whereas g -BC₂ was only recently recognized.

A compound comprising the g -BC₂ structure, Sc₂B_{1.1}C_{3.2}, was discovered by Shi *et al.*¹² In Sc₂B_{1.1}C_{3.2}, the g -BC₂ layers and Sc₂C layers are stacked alternately.^{12,13} The Sc₂C layer is the same as MXene, a single layer of the MAX phases.^{14,15} Sc₂B_{1.1}C_{3.2} can, thus, be regarded as a graphene–MXene complex compound. An incommensurate structure is formed by stacking the BC₂ and Sc₂C layers because they have slightly different unit cell sizes, which gives the compound a large lattice parameter $a = 23.710$ Å. Note that Sc₂B_{1.1}C_{3.2} is thermodynamically stable because it was synthesized via the conventional solid-state reaction and floating zone methods.

Although the precise structure of g -BC₂ was unclear in the experiments,^{12,13} our theoretical study¹⁶ has revealed it to be as shown in Fig. 1, with boron atoms arranged to form a $\sqrt{3} \times \sqrt{3}$ -R30° superlattice. BC₂ may appear to be merely a derivative of the BC _{x} group. However, in contrast to BC and BC₃, BC₂ had not been

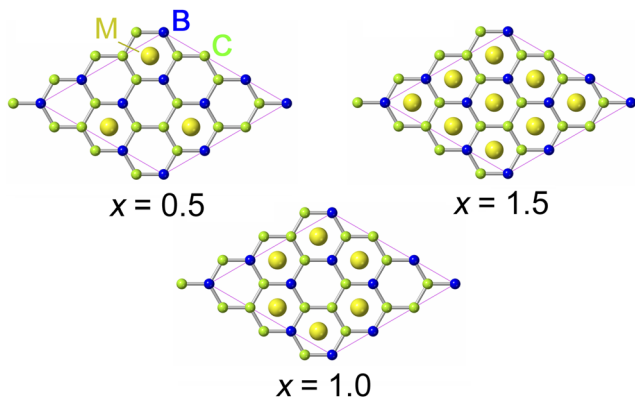


FIG. 1. Structure of BC_2 with alkali metals (M) intercalated (M_xBC_2). B, C, and M are denoted by blue, green, and yellow spheres, respectively.

discovered until our discovery of the $\text{Sc}_2\text{B}_{1.1}\text{C}_{3.2}$ compound in 1999.¹² Even after the discovery, the importance of BC_2 had not been recognized until our recent theoretical study.¹⁶ Therefore, BC_2 is a sort of “missing link” between BC and BC_3 and there have been few other studies on it.

The most stable structure of BC_2 , i.e., the arrangement of B atoms, varies depending on the electric charge of the BC_2 layer itself.¹⁷ When the BC_2 layer has sufficient negative charge, as in $\text{Sc}_2\text{B}_{1.1}\text{C}_{3.2}$, the structure shown in Fig. 1 becomes the most stable. In analogy to graphite intercalation compounds (GICs), we have investigated Li intercalation into $g\text{-BC}_2$.¹⁷ Because alkali metals donate electrons to BC_2 , it is reasonable to study the properties of BC_2 on the basis of the structure in Fig. 1. Intercalated alkali atoms are most stably settled at the hexagonal sites. The calculated intercalation potential for Li indicates that the composition ratio of Li hardly exceeds 1.5 ($\text{Li}_{1.5}\text{BC}_2$) when the hexagonal sites are fully occupied (Fig. 1).¹⁷

GICs containing alkali and alkali-earth metals often exhibit superconductivity at critical temperature (T_c) values in the range of 0.02–11.5 K.¹⁸ In contrast, MgB_2 comprising a graphite-like boron layer has a much higher T_c of 39 K.¹⁹ The higher T_c derives from the fact that the electronic state at the Fermi level has a σ bond component, which couples strongly with bond-stretching phonons.²⁰ Inspired by this, Rosner *et al.* theoretically proposed hole-doped Li_xBC ($x < 1.0$),²¹ and later, Bazhiron *et al.* also reported on $\text{Li}_4\text{B}_5\text{C}_3$ and $\text{Li}_2\text{B}_3\text{C}$ ²² as a potential candidate for high T_c superconductivity. These theoretical studies predicted that the T_c of $\text{Li}_x\text{B}_y\text{C}_z$ compounds could be as high or higher than those of MgB_2 .

Considering these two studies, it is natural to ask whether intercalated $g\text{-BC}_2$ becomes a superconductor as well. In this study, we conducted first-principles calculations to evaluate the T_c values of M_xBC_2 ($\text{M} = \text{Li}, \text{Na}, \text{and K}$) at $x = 0.5, 1.0$, and 1.5 , as shown in Fig. 1. We assumed that Na and K atoms behave like Li, i.e., settle at the hexagonal sites at values of x up to 1.5 .

Interestingly, the electronic structure changes substantially with the value of x . The density of states (DOS) calculated for Li_xBC_2 had a pseudogap, and the Fermi level was located at the bottom of the pseudogap at $x = 1.0$.¹⁷ This suggests that the dominant carrier

changes from holes to electrons as x increases from 0.5 to 1.5 , which would affect how superconductivity emerges in this material. It has been found that T_c for M_xBC_2 depends considerably on x , the mechanism of which will be discussed in detail along with their electronic and phononic structures in Secs. II–IV.

II. COMPUTATIONAL DETAILS

The electronic structures, phonon dispersion curves, and T_c values were calculated using the Quantum ESPRESSO code,²³ based on the density functional theory (DFT) with plane waves and pseudopotentials. The ultrasoft pseudopotentials²⁴ for alkali metals, boron, and carbon were adopted from the library at <http://www.quantum-espresso.org>. The generalized-gradient-approximation (GGA) functional of Perdew–Burke–Ernzerhof (PBE) was employed.²⁵ The energy cutoffs for plane waves were 50 Ry for Li and K and 70 Ry for Na. The cutoffs for the electron density were 400 Ry for Li and 350 Ry for Na and K. These cutoffs were confirmed to provide good convergence of the total energy.

The unit cell used for the calculations was $\sqrt{3} \times \sqrt{3}$ -R30° of the graphite unit cell for all the structures. While having alkali metals intercalated, the stacking of the BC_2 layer was aligned in the z direction, i.e., the xy positions of the B and C atoms were the same in all the BC_2 layers. Thus, the unit cell for the calculations comprised a BC_2 layer and an alkali metal layer, which in total contained two B atoms, four C atoms, and one to three alkali metal atoms corresponding to $x = 0.5$ – 1.5 . k -point sampling was implemented using the Monkhorst–Pack scheme.²⁶ An $(8 \times 8 \times 8)$ mesh was adopted for calculating the electronic structures.

Phonon dispersion curves and Eliashberg spectral functions (α^2F) were calculated using the PHonon package in the Quantum ESPRESSO suite. For the calculation of electron–phonon (EP) coupling coefficients, coarse meshes of $(6 \times 6 \times 6)$ – $(8 \times 8 \times 8)$ were adopted for the phonon k -point grid and fine meshes of $(30 \times 30 \times 30)$ – $(32 \times 32 \times 32)$ were adopted for the Fermi surface calculations. The sum at the Fermi energy was conducted using the interpolation method.²⁷ The T_c values were estimated using the Allen–Dynes formula,²⁸

$$T_c = \frac{\omega_{\log}}{1.2} \exp \left[-\frac{1.04(1 + \lambda)}{\lambda - \mu^*(1 + 0.62\lambda)} \right], \quad (1)$$

$$\omega_{\log} = \exp \left[\frac{2}{\lambda} \int_0^\infty d\omega \frac{\alpha^2 F(\omega)}{\omega} \log \omega \right], \quad (2)$$

$$\lambda = 2 \int_0^\infty d\omega \frac{\alpha^2 F(\omega)}{\omega}, \quad (3)$$

where μ^* is the Coulomb repulsion parameter and was taken as 0.1 in this study.

III. RESULTS AND DISCUSSION

The calculated T_c values for M_xBC_2 ($\text{M} = \text{Li}, \text{Na}, \text{and K}$) are listed in Table I. The T_c values are notably high at $x = 0.5$ for all alkali metals and are much higher than those for GICs such as KC_8 (0.15 K),^{29,30} CaC_6 (11.5 K),³¹ YbC_6 (6.5 K),³¹ LiC_2 (high pressure, 1.9 K),³² and a few-layer graphene intercalate LiC_6 (7.4 K).³³ The T_c

TABLE I. Calculated T_c (K) for M_xBC_2 ($M = \text{Li, Na, and K}$).

M	$x = 0.5$	$x = 1.0$	$x = 1.5$
Li	49.8	0.0	0.6
Na	57.1	0.0	5.6
K	51.6	0.0	1.9

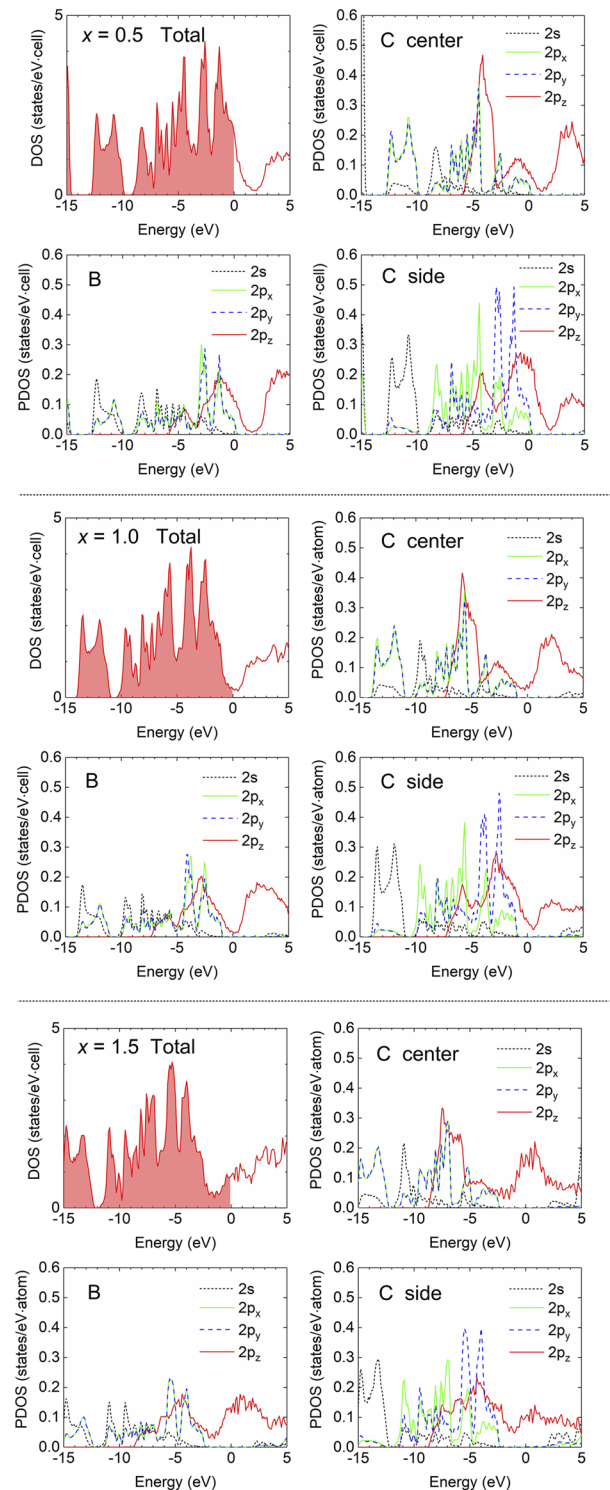
values are rather close to those of MgB_2 (39 K).¹⁹ The emergence of high T_c in graphite-like materials was predicted by Rosner *et al.*, who theoretically demonstrated that the T_c for hole-doped Li_xBC ($x < 1.0$) could rise as high as 100 K.²¹ Bazhironov *et al.* also calculated the T_c values for the $\text{Li}_x\text{B}_y\text{C}_z$ compound and obtained 36.8 K for $\text{Li}_2\text{B}_3\text{C}$ and 16.8 K for $\text{Li}_4\text{B}_5\text{C}_3$.²²

The T_c values for M_xBC_2 vary significantly as x increases from 0.5 to 1.5, during which the materials continue to be metallic, with a finite DOS. The comparison of the T_c values for M_xBC_2 , GICs, and $\text{Li}_x\text{B}_y\text{C}_z$ suggests that the mechanism of superconductivity for M_xBC_2 at $x = 0.5$ may be the same as that for $\text{Li}_x\text{B}_y\text{C}_z$ ^{21,22} and may be the same as that for the GICs at $x = 1.5$.^{29–33}

To elucidate how superconductivity is achieved, the electronic DOSs, phonon dispersion curves, and Eliashberg spectral functions for M_xBC_2 were calculated. Because the electronic structures of M_xBC_2 ($M = \text{Li, Na, and K}$) are similar to each other, the results of the Li case are shown in Figs. 2–5.

Figure 2 shows the total and partial DOSs of Li_xBC_2 ($x = 0.5–1.5$). As mentioned earlier, the total DOSs (top left) have a pseudogap. As x increases from 0.5 to 1.5, the Fermi level (E_f) shifts from below to above the pseudogap. Therefore, the carrier is hole-like at $x = 0.5$, as in the case of $\text{Li}_x\text{B}_y\text{C}_z$,^{21,22} and it is electron-like at $x = 1.5$, as in the case of GICs.^{29–33} The partial DOSs arising from the B and C atoms are shown in Fig. 2, while those from the Li atoms are omitted because they have little contribution to the DOS. At $x = 0.5$, the state at E_f consists of p_x and p_y orbitals of the B and C atoms along with p_z orbitals. The p_x and p_y orbitals in the plane form sp^2 hybridized orbitals that yield σ bonds between atoms. Thus, the state at E_f has the σ bond character, which plays a crucial role in achieving a high T_c , as is the case with $\text{Li}_x\text{B}_y\text{C}_z$ ^{21,22} and MgB_2 .²⁰ In contrast, at $x = 1.0$ and 1.5, it is seen that the state at E_f consists of only p_z orbitals, which indicates that the state has the π bond character as in GICs,^{29–33} and high T_c cannot be expected. Note that at $x = 0.5$, the E_f is located just at the upper end of the p_x and p_y states of B and C. This means that 0.5 is the critical value of x for Li_xBC_2 to have the σ bond character in the state at E_f .

To clarify how the σ and π bond characters appear in the state at E_f , the spatial distributions of DOS at E_f are plotted in Fig. 3. The isosurfaces are plotted in orange, along with the B (blue), C (green), and Li (yellow) atoms. At $x = 0.5$, the state at E_f extends between B and C atoms, exhibiting the σ bond character, and the isosurface also has traits of the p_z orbitals showing that the π bond character is partially mixed, as shown in Fig. 2 (top). In contrast, at $x = 1.0$ and 1.5, the state at E_f has only the π bond character and the overlap between component p_z orbitals is comparatively small. This suggests that the energy of the state at E_f is sensitive to the atomic positions when $x = 0.5$ and much less sensitive when $x = 1.0$ and 1.5, which explains the difference in the strength of

**FIG. 2.** Total and partial densities of states of Li_xBC_2 . Top: $x = 0.5$, middle: $x = 1.0$, and bottom: $x = 1.5$. The Fermi level is set to zero. C center is the carbon atom coordinated with three C atoms, and C side is the carbon atom coordinated to two B atoms and a C atom (see Fig. 1).

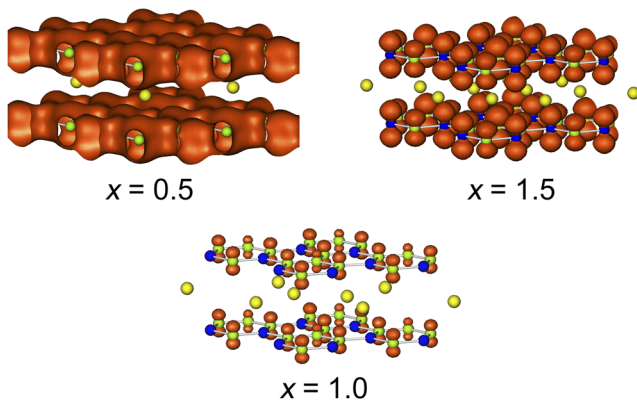


FIG. 3. Spatial distributions of DOS at E_f for Li_xBC_2 . The isosurfaces at 0.05 [states/(Ry cell bohr³)] are plotted in orange. B, C, and Li atoms are denoted by blue, green, and yellow spheres, respectively.

EP coupling. The area of the isosurface at $x = 0.5$ is larger than in the cases of $x = 1.0$ and 1.5 , which would also be favorable for enhancing T_c .

Figure 4 shows the calculated phonon dispersion curves, the DOSs (red), and the Eliashberg spectral functions (α^2F , blue) for Li_xBC_2 . As expected, based on Fig. 3, α^2F is very small at $x = 1.0$, which explains why the material cannot be superconducting at this composition ratio. The Debye frequency at $x = 1.0$ (1340 cm^{-1}) is higher than those at $x = 0.5$ (1295 cm^{-1}) and $x = 1.5$ (1208 cm^{-1}), suggesting that the structure is most stable at $x = 1.0$ because E_f is located at the bottom of the pseudogap. The difference in α^2F between $x = 0.5$ and 1.5 is remarkable. At $x = 0.5$, α^2F is enhanced in the frequency range of 890–970 cm^{-1} , whereas at $x = 1.5$, α^2F in the range of 1050–1200 cm^{-1} is dominant. A qualitative explanation of this is provided based on the analysis of vibrational modes.

Figure 5 illustrates some examples of the vibrational modes of Li_xBC_2 at $x = 0.5$ and 1.5 . These were selected from the region of frequency for each x , where α^2F is enhanced, as mentioned earlier. Frequencies denoted under each figure were calculated at the Γ point. At $x = 0.5$ (left), the vibrations appear to be in the bending modes. This is probably because the σ bond character in the state at E_f (Figs. 2 and 3) originates from sp^2 hybridized orbitals and the bond angle particularly prefers to be 120° . Hence, the change in the bond angle significantly influences the energy of the state leading to strong EP coupling. In contrast, at $x = 1.5$ (right), the vibrations appear to be in the stretching modes. This is understandable because the state at E_f consists of only p_z orbitals of B and C (Figs. 2 and 3), which makes its energy more sensitive to interatomic distance than to bond angle. The small overlap of the p_z orbitals keeps the energy of the state rather unaffected by the atomic positions and causes relatively weak EP coupling.

Thus far, we have theoretically investigated superconductivity in BC_2 . Concerning experiments, Mori *et al.* reported on the electrical resistivity of $\text{Sc}_2\text{B}_{1.1}\text{C}_{3.2}$,³⁴ the compound comprising the BC_2 layer (see Sec. 1). Although the compound is metallic, no superconductivity was observed at temperatures down to 4 K. Based on our previous study,¹⁶ the state at E_f in $\text{Sc}_2\text{B}_{1.1}\text{C}_{3.2}$

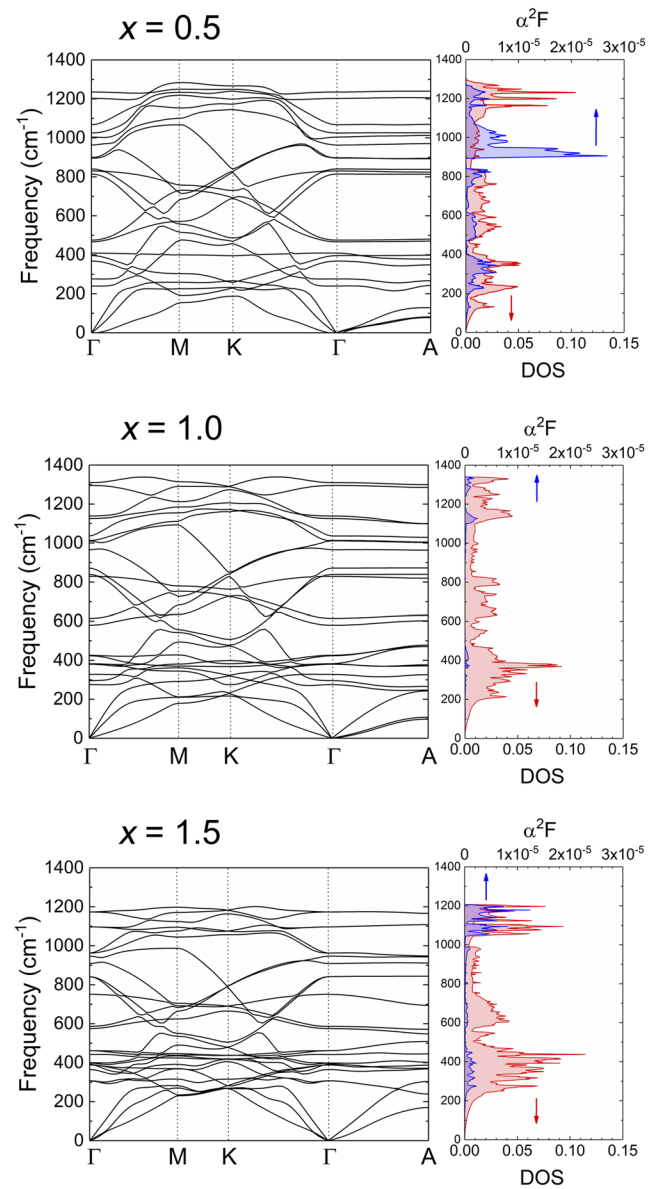


FIG. 4. Phonon dispersion curves, densities of states (DOSs, red), and Eliashberg spectral functions (α^2F , blue) for Li_xBC_2 . Top: $x = 0.5$, middle: $x = 1.0$, and bottom: $x = 1.5$.

mostly consists of Sc $3d$ states. Therefore, the discussion of BC_2 in this paper cannot be applied to superconductivity in $\text{Sc}_2\text{B}_{1.1}\text{C}_{3.2}$. Instead, the superconductivity of the Sc_2C layer (MXene) should be considered.

Another problem that may affect superconductivity is structural disorder. The resistivity of $\text{Sc}_2\text{B}_{1.1}\text{C}_{3.2}$ increased slightly after reaching a minimum at about 75 K, which is interpreted as weak localization due to configurational disorder in the BC_2 layer.³⁴ A similar situation occurred with hole-doped Li_xBC . After Rosner *et al.*'s proposition,²¹ Bharathi *et al.* experimentally searched for

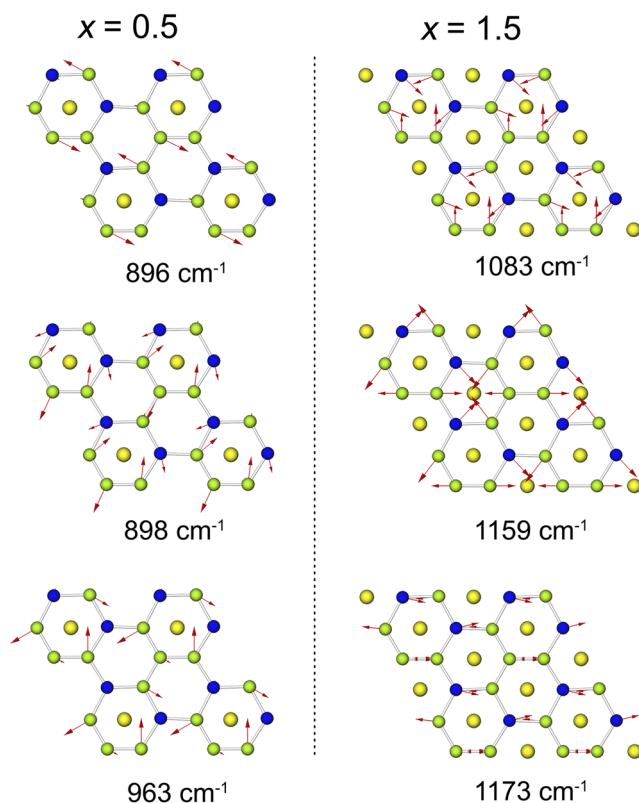


FIG. 5. Examples of vibrational modes for Li_xBC_2 . Left: $x = 0.5$ and right: $x = 1.5$. Red arrows indicate the directions of atomic motion. B, C, and Li atoms are denoted by blue, green, and yellow spheres, respectively.

superconductivity in Li_xBC ($x = 0.4\text{--}1.0$) but was unsuccessful.³⁵ They concluded that the structural disorder in the B–C stacking obstructed the emergence of superconductivity. These experimental findings suggest that B and C atoms can exchange their positions in the BC_x layers without a large increase in the total free energy. Hence, it is crucial to prepare a sample crystal with well-ordered BC_x layers to achieve superconductivity.

In principle, disorder in the BC_x layers increases entropy and accordingly lowers free energy at high temperatures. If the reaction temperature for the synthesis is lowered by choosing appropriate starting materials and catalysts, disorder may be suppressed greatly. As an example, the synthesis of well-ordered α -tetragonal boron has been achieved by using decaborane ($\text{B}_{10}\text{B}_{14}$) as a starting material.³⁶ In this case, hydrogen in decaborane may act as a catalyst that lowers the reaction temperature. Thus, it may be possible to develop an improved method to synthesize well-ordered BC_x .

IV. CONCLUSIONS

The superconductivity of alkali-metal intercalated BC_2 , M_xBC_2 ($\text{M} = \text{Li}, \text{Na}, \text{and K}; x = 0.5\text{--}1.5$), has been investigated using first-principles calculations. The calculated T_c values were substantially high at $x = 0.5$ (49.8–57.1 K), which were higher than those for MgB_2

and close to those predicted for $\text{Li}_x\text{B}_y\text{C}_z$ compounds. The T_c values at $x = 1.5$ were comparatively low and close to those for GICs. The analysis of the partial DOSs revealed that at $x = 0.5$, the state at E_f includes the σ bond character, whereas at $x = 1.5$, the state includes only the π bonds comprising p_z orbitals. The value of 0.5 is the critical value for M_xBC_2 to have a σ bond component. The σ bond character is essential to achieve high T_c values because the σ bond couples strongly with the bending phonon modes of the BC_2 layer. In contrast, the π bond couples weakly with the stretching phonon modes due to the small overlap of the component p_z orbitals, which results in relatively low T_c at $x = 1.0$ and 1.5.

From an experimental point of view, the superconductivity in BC_x layers tends to be suppressed by the configurational disorder of its constituent atoms. Consequently, it is essential to find a way to grow a crystal with well-ordered BC_x layers.

DATA AVAILABILITY

The data that support the findings of this study are available from the corresponding author upon reasonable request.

REFERENCES

- K. S. Novoselov, A. K. Geim, S. V. Morozov, D. Jiang, Y. Zhang, S. V. Dubonos, I. V. Grigorieva, and A. A. Firsov, *Science* **306**, 666 (2004).
- P. Rogl and Materials Science International Team, MSIT Phase diagram of the B–C system: Datasheet from MSI Eureka in SpringerMaterials, Materials Science International Services GmbH, Stuttgart, 2009, http://materials.springer.com/msi/phase-diagram/docs/sm_msi_r_10_023164_02_full_LnkDia2.
- J. Kouvetakis, R. B. Kaner, M. L. Sattler, and N. Bartlett, *J. Chem. Soc., Chem. Commun.* **1986**, 1758.
- B. M. Way, J. R. Dahn, T. Tiedje, K. Myrtle, and M. Kasrai, *Phys. Rev. B* **46**, 1697 (1992).
- B. Ottaviani, A. Derré, E. Grivei, O. A. M. Mahmoud, M.-F. Guimon, S. Flandrois, and P. Delhaës, *J. Mater. Chem.* **8**, 197 (1998).
- C. T. Hach, L. E. Jones, C. Crossland, and P. A. Thrower, *Carbon* **37**, 221 (1999).
- T. Shirasaki, A. Derré, M. Ménétrier, A. Tressaud, and S. Flandrois, *Carbon* **38**, 1461 (2000).
- Z. Weng-Sieh, K. Cherrey, N. G. Chopra, X. Blase, Y. Miyamoto, A. Rubio, M. L. Cohen, S. G. Louie, A. Zettl, and R. Gronsky, *Phys. Rev. B* **51**, 11229 (1995).
- H. Yanagisawa, T. Tanaka, Y. Ishida, M. Matsue, E. Rokuta, S. Otani, and C. Oshima, *Phys. Rev. Lett.* **93**, 177003 (2004).
- M. Wörle and R. Nesper, *J. Alloys Compd.* **216**, 75 (1994).
- M. Wörle, R. Nesper, G. Mair, M. Schwarz, and H. G. von Schnering, *Z. Anorg. Allg. Chem.* **621**, 1153 (1995).
- Y. Shi, A. Leithe-Jasper, L. Bourgeois, Y. Bando, and T. Tanaka, *J. Solid State Chem.* **148**, 442 (1999).
- M. Onoda, Y. Shi, A. Leithe-Jasper, and T. Tanaka, *Acta Crystallogr., Sect. B: Struct. Sci.* **57**, 449 (2001).
- M. Naguib, M. Kurtoglu, V. Presser, J. Lu, J. Niu, M. Heon, L. Hultman, Y. Gogotsi, and M. W. Barsoum, *Adv. Mater.* **23**, 4248 (2011).
- S. Kumar and U. Schwingenschlögl, *Phys. Rev. B* **94**, 035405 (2016).
- W. Hayami and T. Tanaka, *J. Solid State Chem.* **254**, 144 (2017).
- W. Hayami and T. Tanaka, *J. Solid State Chem.* **269**, 113 (2019).
- R. P. Smith, T. E. Weller, C. A. Howard, M. P. M. Dean, K. C. Rahnejat, S. S. Saxena, and M. Ellerby, *Physica C* **514**, 50 (2015).
- J. Nagamatsu, N. Nakagawa, T. Muranaka, Y. Zenitani, and J. Akimitsu, *Nature* **410**, 63 (2001).
- Y. Kong, O. V. Dolgov, O. Jepsen, and O. K. Andersen, *Phys. Rev. B* **64**, 020501 (2001).

- ²¹H. Rosner, A. Kitaigorodsky, and W. E. Pickett, *Phys. Rev. Lett.* **88**, 127001 (2002).
- ²²T. Bazhiron, Y. Sakai, S. Saito, and M. L. Cohen, *Phys. Rev. B* **89**, 045136 (2014).
- ²³P. Giannozzi, S. Baroni, N. Bonini, M. Calandra, R. Car, C. Cavazzoni, D. Ceresoli, G. L. Chiarotti, M. Cococcioni, I. Dabo, A. Dal Corso, S. Fabris, G. Fratesi, S. de Gironcoli, R. Gebauer, U. Gerstmann, C. Gougoussis, A. Kokalj, M. Lazzeri, L. Martin-Samos, N. Marzari, F. Mauri, R. Mazzarello, S. Paolini, A. Pasquarello, L. Paulatto, C. Sbraccia, S. Scandolo, G. Sclauzero, A. P. Seitsonen, A. Smogunov, P. Umari, and R. M. Wentzcovitch, *J. Phys.: Condens. Matter* **21**, 395502 (2009); [arXiv:0906.2569](https://arxiv.org/abs/0906.2569).
- ²⁴D. Vanderbilt, *Phys. Rev. B* **41**, 7892 (1990).
- ²⁵J. P. Perdew, K. Burke, and M. Ernzerhof, *Phys. Rev. Lett.* **77**, 3865 (1996).
- ²⁶H. J. Monkhorst and J. D. Pack, *Phys. Rev. B* **13**, 5188 (1976).
- ²⁷M. Wierzbowska, S. de Gironcoli, and P. Giannozzi, "Origins of low- and high-pressure discontinuities of T_c in niobium," [arXiv:cond-mat/0504077v2](https://arxiv.org/abs/cond-mat/0504077v2) (2006).
- ²⁸P. B. Allen and R. C. Dynes, *Phys. Rev. B* **12**, 905 (1975).
- ²⁹N. B. Hannay, T. H. Geballe, B. T. Matthias, K. Andres, P. Schmidt, and D. MacNair, *Phys. Rev. Lett.* **14**, 225 (1965).
- ³⁰Y. Koike, H. Suematsu, K. Higuchi, and S. Tanuma, *Physica B+C* **99**, 503 (1980).
- ³¹T. E. Weller, M. Ellerby, S. S. Saxena, R. P. Smith, and N. T. Skipper, *Nat. Phys.* **1**, 39 (2005).
- ³²I. T. Belash, A. D. Bronnikov, O. V. Zharikov, and A. V. Pal'nichenko, *Solid State Commun.* **69**, 921 (1989).
- ³³A. P. Tiwari, S. Shin, E. Hwang, S. Jung, T. Park, and H. Lee, *J. Phys.: Condens. Matter* **29**, 445701 (2017).
- ³⁴T. Mori, M. Tansho, Y. Onoda, Y. Shi, and T. Tanaka, *Phys. Rev. B* **62**, 7587 (2000).
- ³⁵A. Bharathi, S. Jemima Balaselvi, M. Premila, T. N. Sairam, G. L. N. Reddy, C. S. Sundar, and Y. Hariharan, *Solid State Commun.* **124**, 423 (2002).
- ³⁶E. A. Ekimov, Y. B. Lebed, N. Uemura, K. Shirai, T. B. Shatalova, and V. P. Sirostinkin, *J. Mater. Res.* **31**, 2773 (2016).